

# Dielectric TM-Mode Y-Shaped Doublet Structure

DANIEL MIEK <sup>1</sup> (Member, IEEE), PATRICK BOE <sup>1</sup> (Graduate Student Member, IEEE),  
FYNN KAMRATH <sup>1</sup> (Graduate Student Member, IEEE), KENNET BRAASCH <sup>1</sup>, WOLFGANG TAUTE,  
AND MICHAEL HÖFT <sup>1</sup> (Senior Member, IEEE)

(Regular Paper)

Department of Electrical and Information Engineering, Kiel University, 24143 Kiel, Germany

CORRESPONDING AUTHOR: Michael Höft (e-mail: mh@tf.uni-kiel.de).

This work was supported by DFG within the funding programme Open Access Publikationskosten.  
This work did not involve human subjects or animals in its research.

**ABSTRACT** This paper discusses dielectric TM-mode filters based on high permittivity Y-shaped ceramics. It is shown that this type of ceramic operates as a dual-mode resonator and therefore contributes two reflection zeros as well as one transmission zero (TZ) to the filter response. Hence, it can be interpreted as a doublet structure and used for the realization of quasi-elliptical filter responses of different order. The dual-mode resonator can be used in multiple different filter set-ups: On the one hand, a combination with classical TM<sub>010</sub>-mode resonators is possible to allow the realization of TZs in an in-line filter configuration without using cross-coupling apertures. Therefore, negative or diagonal cross-couplings, which are often difficult to realize and handle, can be avoided. On the other hand, several Y-shaped ceramics can be coupled directly with each other to increase the number of TZs to  $n_{fz} = n/2$ , where  $n$  is the order of the filter. Finally, it is shown that even a combination with extracted pole elements is realizable. Prototypes based on modular segments are manufactured as proof of concept.

**INDEX TERMS** Doublet, dual-Mode, extracted pole, TM-mode, Y-shaped ceramic.

## I. INTRODUCTION

Dielectric resonator filters are a current research topic as they reveal several advantages in most communication systems with respect to cost, volume, mass and electrical performance compared to other filter types. They offer a substantial size reduction in the lower gigahertz regime compared to waveguide filters and feature high Q-factors depending on the ceramic material used for fabrication [1], [2]. Filters based on dielectric resonators can be realized by using different modes of operation, whereby in many cases TE- as well as TM-mode resonators are used. A typical TE-mode ceramic is shown in Fig. 1(a). The ceramic with high permittivity is placed on a support structure with lower permittivity. In the fundamental TE<sub>01δ</sub>-mode, the electric field rotates inside the ceramic and reveals advantageous properties with respect to the achievable quality factor. Otherwise, the spurious-free range is often comparably small and higher order modes are

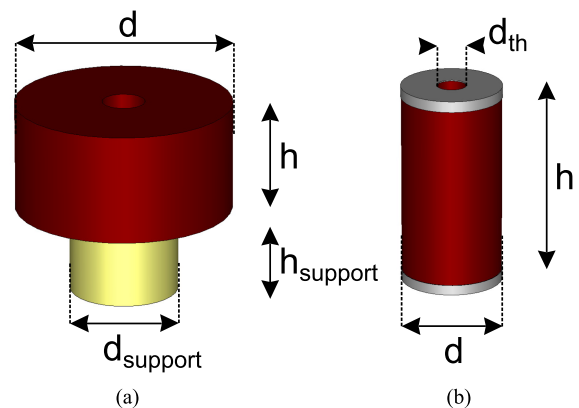


**FIGURE 1.** (a) Principal drawing of a TE-mode resonator placed on a low permittivity support material and (b) principal drawing of a TM-mode resonator with silver-plated top and bottom surfaces.

comparatively close. One solution to overcome this drawback is to combine different resonator types / modes of operation or to use a wideband lowpass filter in cascade with the bandpass filter [3], [4], [5], [6]. TM-mode filters are a well-known alternative [7], [8], [9]. A typical ceramic in  $TM_{010}$ -mode configuration is shown in Fig. 1(b). In the fundamental mode, the electric field is guided between both silver-plated ends, which are provided here for soldering purposes. Disadvantageously, TM-mode resonators require a suitable contact between the ceramic material and the surrounding metallic housing, which has the most impact on the insertion loss of a filter.

Different approaches are known for the realization of quasi-elliptical filter responses in dielectric TM-mode filters. The most forward approach is to use single-mode resonators and to employ cross-coupling apertures between the resonators as designated by the coupling matrix to achieve the desired filter response / TZ positions [10], [11]. However, the realization and tuning of the (possibly negative) cross-coupling might be complicated due to mechanical reasons. Another option is to use the recently discussed extracted zero technique, where TZs can be generated using singly terminated resonators, which are excited close to the source and / or load port [12], [13]. Disadvantageously, only a TZ is included in the filter response without introducing a further reflection zero. Therefore, the footprint is increased by at least one resonator without increasing the filter order.

In this paper, a dielectric TM-mode doublet structure based on a Y-shaped ceramic is discussed. As a characteristic property of a doublet, it contributes two reflection zeros as well as one transmission zero to the filter response [14]. The ceramic itself was first proposed in [15] as a dual-mode resonator. However, the paper is limited to the realization of a second order filter and the advantages of the structure are not fully exploited. This paper therefore focuses on the realization of higher order filters based on the combination of different resonator types. The advantages of the Y-shaped ceramic can be summarized as follows:

- All branches of the ceramic are bent to a common base plate. Contact problems are therefore minimized compared to standard TM-mode ceramics, which require a contact to both, bottom and cover.
- The resonator introduces two reflection zeros as well as one TZ and is therefore proposed as a ceramic TM-mode doublet.
- It can be used within an in-line filter configuration by coupling to standard TM-mode resonators. Cross-coupling apertures might therefore be avoided.
- In addition to the points mentioned above, several Y-shaped ceramics can be coupled as well, leading to a maximum number of  $n_{fz} = n/2$  TZs, where  $n$  is the filter order. Furthermore, a combination with extracted pole segments is possible.

This paper is organized as follows: Section II reviews and expands the investigation of the basic second order dual-mode resonator from [15]. Section III presents the incorporation of the doublet in an all-pole filter response, resulting in a fourth

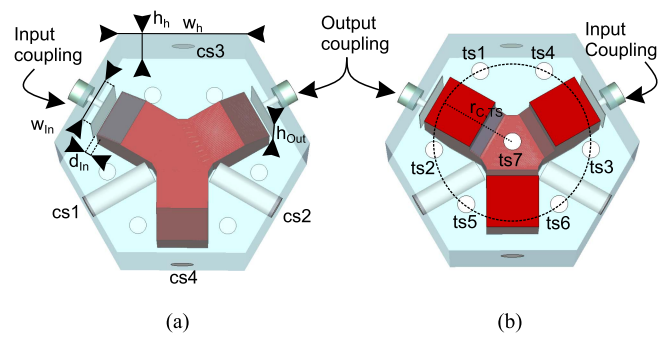


**FIGURE 2.** Second order filter including the input / output coupling as well as tuning screws: (a) top view and (b) bottom view.

order filter. Measurement results are presented based on a modular and flexible prototype. Section IV shows, that several doublets can be coupled with each other. In Section V the combination of the doublet with two extracted pole sections is discussed, resulting in a fourth order filter as well. Finally, Section VI summarizes and concludes this paper.

## II. SECOND ORDER DUAL-MODE RESONATOR

### A. BASIC INVESTIGATIONS

The basic set-up is shown in Fig. 2(a) (top view) and (b) (bottom view). The Y-shaped ceramic is placed in a hexagonal cavity with height  $h_h = 25$  mm and width  $w_h = 22$  mm. The dimensions of the Y-shaped ceramic are identical to those discussed in [15] and are hence not repeated here. In the standard configuration, each branch of the ceramic has the same dimensions. Therefore, it reveals a  $120^\circ$  rotational symmetry. The ceramic is assumed to have a relative permittivity of  $\epsilon_r = 42.4$ .

Four screws denoted as cs1-cs4 are included at the side-walls of the set-up in order to tune the resonances of the Y-shaped ceramic. Additionally, six tuning screws (ts1-ts6) distributed on a circle with radius  $r_{c,TS} = 13.6$  mm can be inserted from the bottom of the hexagonal-shaped cavity. These screws are preliminary used in the measurement set-up in order to have additional degrees of freedom in the tuning process rather than in simulations. The input and output couplings are realized by inductive plate couplings [11]. The plates have a width of  $w_{in/out}$ , height  $h_{in/out}$  and distance to the ceramic branch  $d_{in/out}$ . In case of a second order filter, two of the three branches are excited by the inductive coupling plates.

By initially neglecting all screws as well as the input / output coupling, the proposed configuration reveals a  $120^\circ$  rotational symmetry with respect to the center. The electric field distribution of the arising modes can be calculated analytically as proposed by the branch-vector approach in [16], [17]. For this configuration, two modes at the same frequency result with the electric field distribution as shown in Fig. 3. The modes can be distinguished by their symmetry plane: The mode in Fig. 3(a)/(c) has a magnetic symmetry plane whereas the mode in (b)/(d) exhibits an electric symmetry plane. In

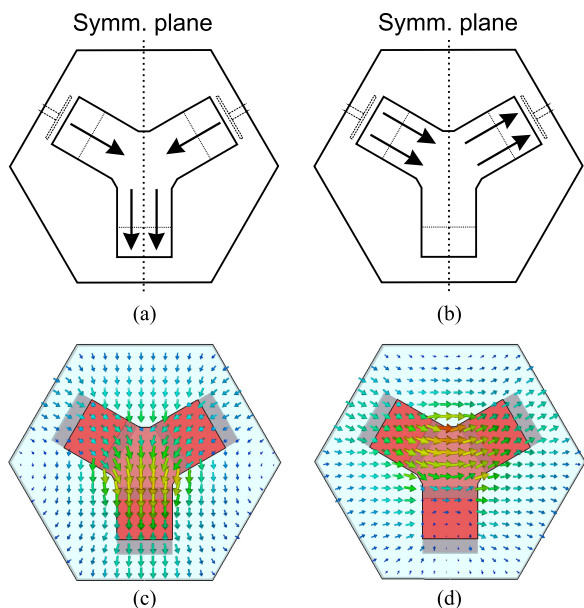


**FIGURE 3.** Electric field distribution of the eigenmodes in the Y-shaped ceramic resonator: (a) / (c) mode with magnetic symmetry plane and (b) / (d) mode with electric symmetry plane. The input / output couplings in the principal drawings in (a) / (b) are only shown for comparison purposes with Fig. 2 but are not included in this investigation.

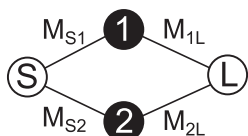


**FIGURE 4.** Topology of the second order filter responses with respect to Fig. 5. The coupling factors are as follows:  $M_{S1} = M_{1L} = 0.545$ ,  $-M_{S2} = M_{2L} = 1.183$ ,  $M_{11} = 1.577$ ,  $M_{22} = -1.356$  in case of Fig. 5(a) and  $M_{S1} = M_{1L} = 0.687$ ,  $-M_{S2} = M_{2L} = 1.042$ ,  $M_{11} = -1.658$ ,  $M_{22} = 1.534$  in case of Fig. 5(b).

the latter case, there is no electric field in the lower branch. For the given dimensions, the desired resonant modes arise at 2019 MHz whereas the first spurious mode can be identified as a cavity mode at 2829 MHz. Due to the  $120^\circ$  rotational symmetry, the modes might be rotated pairwise. With respect to Fig. 2, the dual-mode resonator must be tuned in a way that both modes can be excited from the source/load port. The resulting topology for this case is a transversal array of second order as shown in Fig. 4 [18].

A filter response of second order can be obtained by including the input / output coupling as well as all tuning screws to the simulation model. Fig. 5 shows two different simulated S-Parameter results. By choosing e.g. only the screw cs3 for tuning the filter response, a TZ below the passband occurs at normalized frequency  $f_{TZ,LP} = -j2.37$ . The appearance of the TZ might be explained by means of Fig. 3. The electric field components of the mode with magnetic symmetry (Fig. 3(a)/(c)) are guided to the symmetry line from the source and load ports point of view. Otherwise, as shown in Fig. 3(b)/(d), the electric field of the mode with electrical

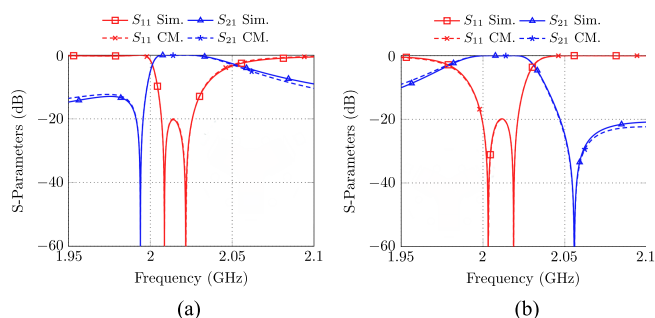


**FIGURE 5.** Simulated S-Parameters in comparison to coupling matrix representation for (a) the case with a TZ below the passband and (b) the case with a TZ above the passband.

symmetry plane has opposite directions at the source and load ports. Therefore, one coupling factor must be interpreted negative in the transversal array coupling matrix description. Furthermore, as the electric field of both modes reveal different intensity in the branches which are excited by the source / load ports, the coupling factors differ in their absolute values which cause the occurrence of a TZ [19], [20]. By using only cs4 instead of cs3, the TZ can be shifted to a normalized frequency of  $f_{TZ,LP} = -j3.58$ . It is worth mentioning, that the use of tuning screws from the sidewalls decrease the frequency of the first spurious mode. In case of Fig. 5(a), the first spurious mode arises at 2602 MHz.

By using the tuning screws cs1 and cs2 whose length is changed symmetrically, the TZ can also be moved to the other side of the passband to the normalized frequency  $f_{TZ,LP} = j4.107$  (compare Fig. 5(b)). The dual-mode resonator therefore shows the zero-shifting property [21] as already discussed in [15]. In this case, the first spurious mode arises at 2460 MHz. The spurious mode behaviour might be improved by using a Y-shaped resonator with holes in each of its three feet. The tuning screws might then be inserted from the bottom instead of from the sidewalls, which shifts the first spurious mode to higher frequencies. However, in this paper the ceramics shown in Fig. 2 or [15] are used due to their availability.

## B. COUPLING FACTOR INVESTIGATION

The results from Fig. 5 motivate the implementation of a coupling factor study. Considering the matched filter response from Fig. 5(b) as well as the associated coupling factors of a second order transversal array filter (compare Fig. 4), the influence of the variation of tuning screw depths is investigated and expressed in variations of coupling factors. The results are shown in Fig. 6.

In Fig. 6(a) cs4 is varied in depth and the effect on all coupling factors is visualized. As the mode with electric symmetry plane has no field portions in the corresponding branch (compare Fig. 3(a)), only the mode with magnetic symmetry plane is influenced by this operation. This mode can therefore be associated with the coupling factor  $M_{11}$ , as all other coupling factors remain constant. In Fig. 6(b) the

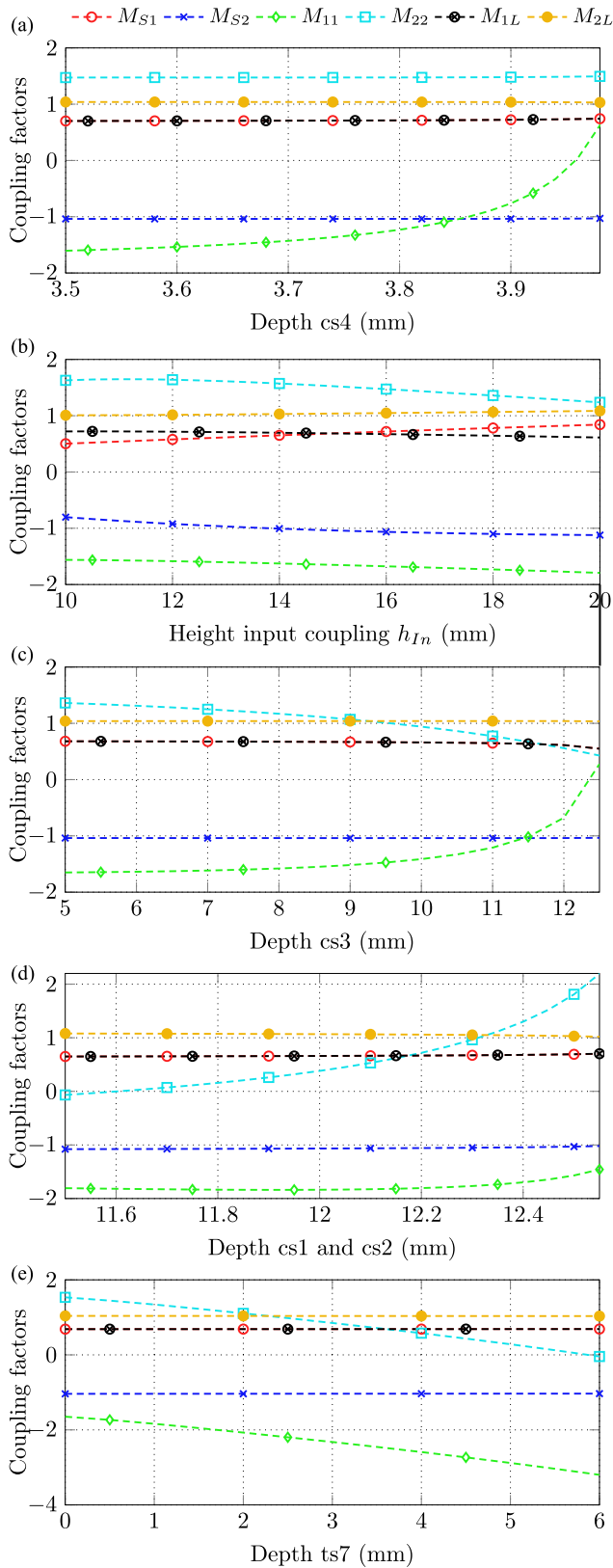


**FIGURE 6.** Coupling factor study of the filter set-up from Fig. 2 with a TZ above the passband in dependency from: (a) depth of screw cs4, (b) height of the input coupling, (c) depth of screw cs3, (d) depth of the screws cs1 and cs2 (symmetrically tuned) and (e) depth of screw ts7.

height of the input coupling plate  $h_{In}$  is varied. The absolute values of the coupling factors  $M_{S1}$  and  $M_{S2}$  increase for growing height of the coupling plate. Furthermore, loading effects on both resonances as well as small variations of the output coupling factors can be recognized as well. The depth of cs3 is varied in Fig. 6(c). This coupling screw is not used in the initial simulation of Fig. 5(b). For an increasing screw depth, the coupling factors show an opposite behavior, since the self-coupling  $M_{22}$  decreases while  $M_{11}$  increases. This observation enables the zero shifting property, where it is required that both self-couplings exchange their signs. By varying cs1 and cs2 (symmetrically), both self-couplings  $M_{11}$  and  $M_{22}$  increase while all other coupling factors maintain constant, which is shown in Fig. 6(d). The tuning screw ts7, which is localized on the bottom of the cavity below the Y-shaped ceramic, allows with increasing depth, that both self-couplings  $M_{11}$  and  $M_{22}$  decrease synchronously (compare Fig. 6(e)). This property is useful, if exemplary the bandwidth of the fourth order filter proposed in the next section should be increased. Loading effects might then be compensated, as the resonance frequency of both modes can be increased synchronously.

A prototype as well as measurement results of a second order filter are outlined in [15], wherefore this paper discusses the realization of higher order filters based on Y-shaped ceramics.

### III. DOUBLET IN IN-LINE FILTERS

#### A. BASIC INVESTIGATIONS AND FILTER DESIGN

A meaningful application of the proposed dual-mode resonator is the incorporation in in-line filter configurations in order to realize TZs without using cross-coupling apertures. A fourth order filter model is shown in Fig. 7(a) while the associated coupling topology is depicted in (b). The filter model basically consists of three elements, namely two TM-mode resonators as well as a doublet realized as a Y-shaped ceramic. The input and output couplings are realized as inductive plates, which couple to the TM single-mode dielectric resonators [11]. In agreement with Fig. 1(b), the rods have an outer diameter of  $d = 10$  mm, a height of  $h = 20$  mm and a hole for the insertion of tuning screws with  $d_{th} = 3$  mm diameter. The relative permittivity is assumed to be similar to that of the Y-shaped ceramic. The  $TM_{010}$ -mode resonators and the Y-shaped ceramic are designed to have a similar center frequency. Therefore, a coupling of both elements is possible. The TM-mode rods are coupled via inductive coupling apertures with diameter  $w_{ca} = 12$  mm and depth  $d_{ca} = 4$  mm to a branch of the Y-shaped ceramic. The inter-resonator coupling can be adjusted using tuning screws inside the iris. The dual-mode resonator reveals the same tuning options as denoted in Fig. 2.

The coupling topology is shown in Fig. 7(b). The source and load ports are both coupled to TM single-mode resonators with couplings factors  $M_{S1}$  and  $M_{4L}$ , respectively. The  $TM_{010}$ -mode resonators couple to both modes of the Y-shaped

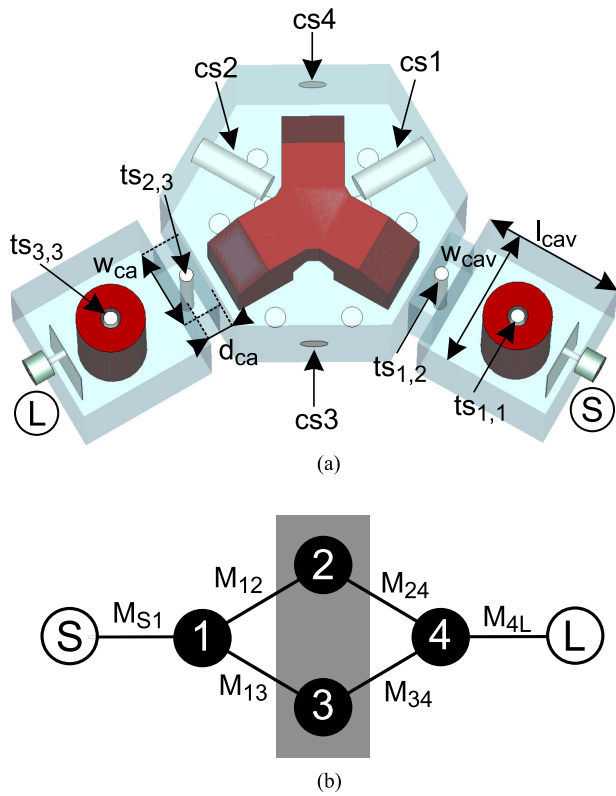


**FIGURE 7.** Fourth order filter consisting of two  $TM_{010}$ -mode resonators (with  $l_{cav} = w_{cav} = 21$  mm) and a Y-shaped doublet: (a) simulation model and (b) associated coupling topology.

ceramic simultaneously (compare Fig. 3), while it is assumed that there is no coupling between the modes of the doublet (compare Fig. 4).

The filter design procedure can be divided into different steps. The determination of the external quality factor of the first / last resonator is well known in the literature for the case that single-mode resonators are used [11], [22]. The depths of the tuning screws cs1-cs4 in the doublet structure are used to place the TZ either above or below the passband (compare Fig. 5). In the initial simulation of the fourth order filter, the depth of the tuning screws might be adopted from the simulations in Fig. 5. The  $TM_{010}$ -mode ceramics couple two modes in the Y-shaped dual-mode resonator simultaneously. In the initial simulation the depths of the screws  $ts_{1,2}$  and  $ts_{2,3}$  should be chosen in a way to achieve a sufficient coupling strength. Fig. 8 shows a plot of the coupling factors  $M_{12}$  and  $M_{13}$  in dependency from the screw depth  $ts_{1,2}$ . The coupling factors can be obtained by coupling matrix extraction techniques while simulating the complete filter with varying tuning screw depth. In the case presented here, the reference coupling matrix is adapted to a return loss level of  $RL = 23$  dB and reveals a TZ above the passband at a normalized frequency of  $f_{TZ,LP} = j2.24$ . From this specifications, the coupling matrix in Table 1 can be derived. As visualized in Fig. 8, the desired coupling factors can be achieved using a

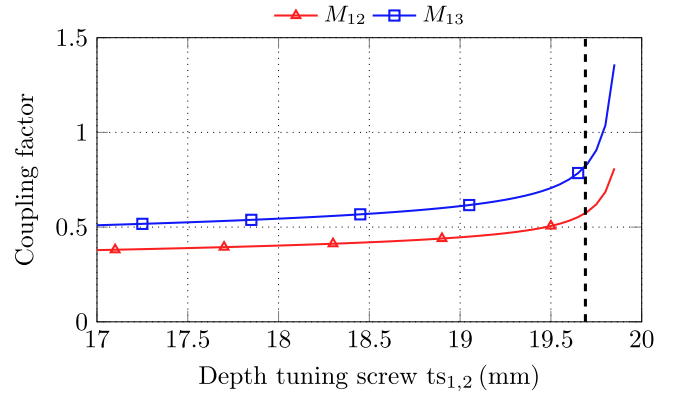


**FIGURE 8.** Coupling factors  $M_{12}$  and  $M_{13}$  in dependency from the depth of the screw  $ts_{1,2}$  for the filter presented in Fig. 7. The vertical dashed line visualizes the depth, at which the desired coupling factors in Table 1 are achieved.

**TABLE 1.** Coupling Matrix of the Filter Topology in Fig. 7(b) With One TZ Above the Passband at Normalized Frequency  $f_{TZ,LP} = j2.24$  and a Return Loss Level of  $RL = 23$  dB

-	S	1	2	3	4	L
S	0.0	1.104	0.0	0.0	0.0	0.0
1	1.104	0.049	0.561	0.809	0.0	0.0
2	0.0	0.561	-0.895	0.0	-0.561	0.0
3	0.0	0.809	0.0	0.561	0.809	0.0
4	0.0	0.0	-0.561	0.809	0.049	1.104
L	0.0	0.0	0.0	0.0	1.104	0.0

screw depth of approx. 19.7 mm (compare vertical dashed line).

As can be seen from Fig. 8, the coupling factors  $M_{12}$  and  $M_{13}$  (and similarly  $M_{24}$  and  $M_{34}$ ) cannot be controlled independently from each other. This leads to the restriction, that the TZ cannot be moved freely along the frequency axis. However, the Y-shaped ceramic resonator is proposed as a building block in the filter design. It can be used in combination with other techniques which provide TZs and might reduce the number of (negative) cross-couplings in a filter set-up. Additional TZs might also be realized using e.g. the extracted pole [23], [24] or the extracted zero technique [12], [13]. Furthermore, it is possible to couple several Y-shaped resonators with each other to achieve a high selectivity either below or above the passband. This is discussed in Section IV.

It is further worth to mention that with respect to Fig. 8, the bandwidth of the fourth order filter might be varied. An increase of the bandwidth can exemplarily be achieved, if the depth of the tuning screws  $ts_{1,2}$  and  $ts_{2,3}$  as well as cs1 and cs2 (in case that the TZ is placed above the passband) is increased. Furthermore, the input/output coupling strength must be enlarged using the distance or size of the coupling plate. Due to loading effects, the tuning screw  $ts_7$  centrally located below the Y-shaped ceramic must be increased in depth as well. This screw increases the resonance frequency of both eigenmodes and therefore compensates the loading effects. However, a

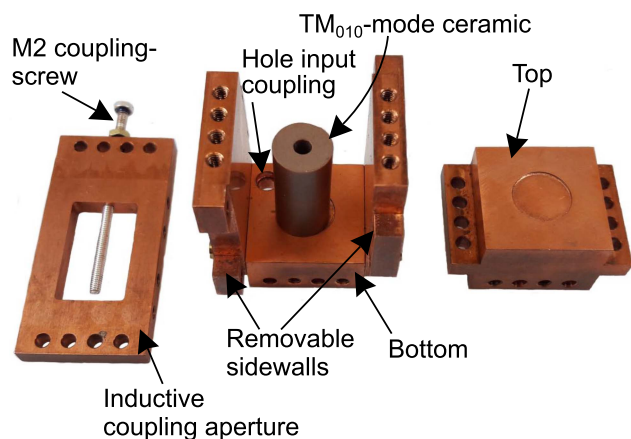


**FIGURE 9.** TM-mode segment. Left: Inductive coupling aperture with M2 tuning screw. Center: Bottom and two sidewall-elements of a TM-mode segment. A ceramic is placed in the center. Right: Top of the TM-mode segment.

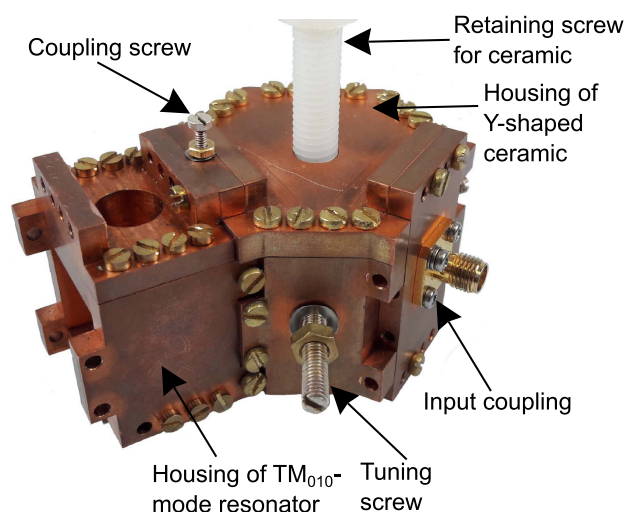


**FIGURE 11.** Assembled components from Fig. 9 and Fig. 10 resulting in a third order segment.

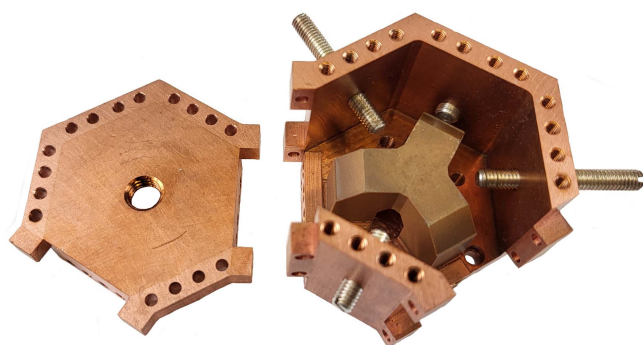


**FIGURE 10.** Doublet segment. Left: Cover with M8 thread. Right: Housing of the Y-shaped ceramic with tuning screws assembled.

decrease of the resonance frequency is not possible, wherefore the dimensions of the ceramic must be properly selected in the design stage of the filter.

## B. MANUFACTURED PROTOTYPE AND MEASUREMENT RESULTS

The filter model from Fig. 7 is manufactured as proof of concept. A modular design was chosen in order to allow the realization of different filter configurations presented in this paper without manufacturing several prototypes. A TM single-mode resonator segment as well as the inductive coupling aperture are shown in Fig. 9. The segments are designed in a way that either a combination with further TM-mode resonators or doublet structures is possible. The TM single-mode resonator segment is constructed for an easy and simple manufacturing and reduces the time-consuming machining of copper to a minimum. It therefore consists of a bottom part, two removable sidewalls and a top, which are mounted together by screws. The bottom as well as the top reveal a recess to correctly align the TM single-mode ceramic within the housing. The ceramic is then clamped between the bottom and the top [8]. A thread for inserting a tuning screw is located

in the center of the bottom element. Additionally, the blend apertures between the resonators can be exchanged as well. The input / output coupling plate is connected to the SMA port through a wire and its orientation can be adjusted with a screw using a designated hole (compare [11]). The segment is then terminated by a plate with an SMA connector mounted on the outside. The realization of the input coupling element is exemplary shown in Fig. 11.

The dual-mode resonator segment is shown in Fig. 10. It consists of a cover with a centered M8 thread, in which a plastic screw is introduced to clamp the Y-shaped ceramic within the housing. Alternatively, it is also possible to solder the silver-plated ends of the ceramic with the housing. The Y-shaped ceramic itself is fabricated conventionally, i.e. a ceramic powder with the desired electrical properties is mixed with a binder. Afterwards, this mixture is pressed in a suitable form and subsequently sintered. Due to the shrinkage of the ceramic in the sintering process, the negative form must be properly enlarged, which may require some iterations. The hexagonal-shaped cavity provides threads for the tuning screws at positions shown in Fig. 2. Two openings in the sidewall are designed to allow a coupling with either a TM-mode segment or further doublets. Additionally, these openings can be closed with a plate and used as an input / output coupling. An assembled third order filter consisting of a doublet as well as a TM single-mode resonator segment is shown in Fig. 11. The TM single-mode ceramics are manufactured using the same process as the Y-shaped ceramics. In comparison, cylindrical TM single-mode ceramics can be manufactured easily and are often used in the literature [11], [25].

Two different measurements are accomplished by investigating the fourth order filter set-up from Fig. 7 using the modular segments. In Fig. 12 the filter is tuned to achieve a return loss level of  $RL = 22$  dB between the band edges at  $f_1 = 2056$  MHz and  $f_2 = 2089$  MHz. The TZ arises at

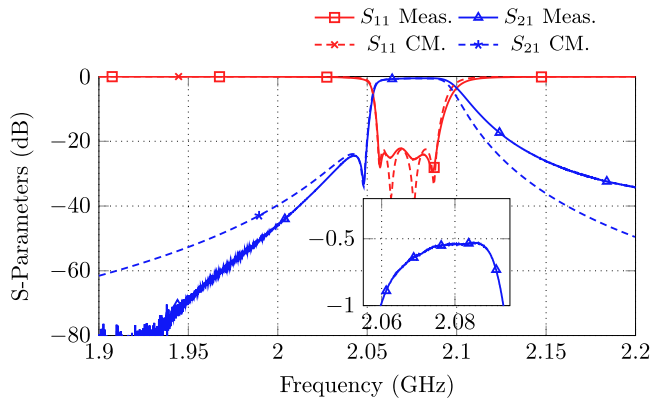


**FIGURE 12.** S-Parameters of a fourth order filter consisting of two TM single-mode resonators and a doublet with one TZ below the passband.

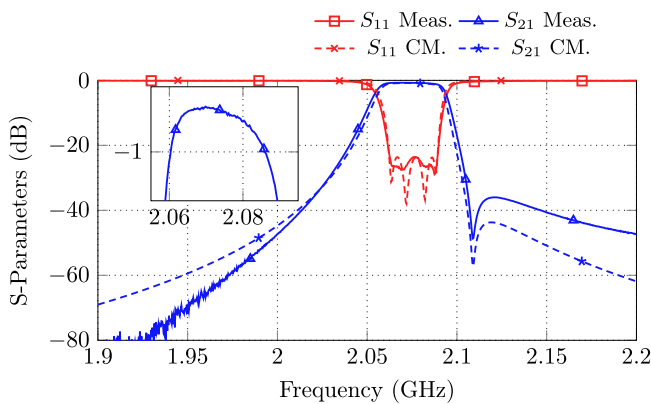


**FIGURE 13.** S-Parameters of a fourth order filter consisting of two TM single-mode resonators and a doublet with one TZ above the passband.

a normalized frequency of  $f_{TZ,LP} = -j1.49$ . The measurement results are presented in comparison with a coupling matrix representation, from which an unloaded quality factor of  $Q_u \approx 1730$  can be estimated [26]. The most significant loss mechanisms include the modular set-up, which consists of multiple parts, as well as the plastic screw which is used to provide the contact between the housing and the Y-shaped ceramic (see Fig. 11).

Furthermore, deviations between the measurement and the coupling matrix representation far out of band appear. These deviations are attributed to the frequency dependency of the couplings. While all couplings are assumed frequency independent in the coupling matrix approach, there is a dispersive characteristic in physical coupling apertures. Besides, spurious modes above the passband reveal further coupling paths which might contribute to the deviations.

By varying the depth of the tuning screws within the doublet, the TZ can be moved to the other side of the passband. The measurement results are shown in Fig. 13. The filter is matched to a return loss level of  $RL = 23$  dB between the band edges at  $f_1 = 2062.2$  MHz and  $f_2 = 2089.3$  MHz. The TZ arises at a normalized frequency of  $f_{TZ,LP} = j2.431$ . In this measurement, an unloaded quality factor of  $Q_u \approx 1600$

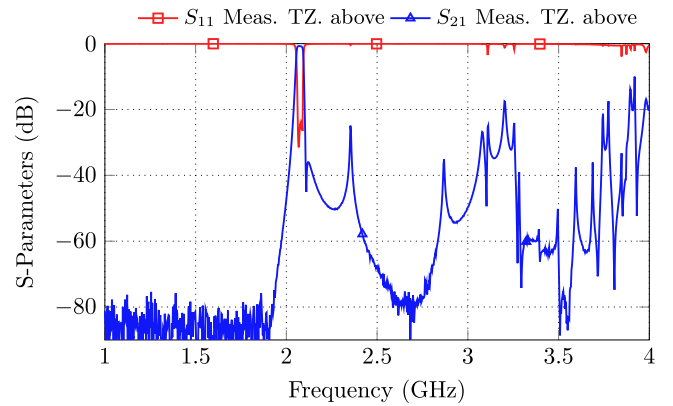


**FIGURE 14.** Spurious mode performance of the measurement in Fig. 13.

can be achieved. The degraded Q-factor compared to the first measurement might be explained by the tuning screw depths, which are required to achieve the presented results. In the case where the TZ arises below the passband, mainly cs3 is placed close to the ceramic. However, in the case where the TZ is located above the passband, cs1 as well as cs2 need to be inserted deeply. The spurious mode performance of the latter measurement is shown in Fig. 14. The first spurious mode arises at 2350 MHz and can be associated with the tuning screws, which are deeply inserted. As discussed in Section II, improvements might be obtained if the Y-shaped ceramic has holes in the feet which allow the insertion of tuning screws from the bottom.

## IV. COMBINATION OF SEVERAL DOUBLETS

### A. FILTER SET-UP

Apart from the coupling between a Y-shaped ceramic and  $TM_{010}$ -mode resonators, it is also possible to couple multiple Y-shaped resonators. Fig. 15 shows the simulation model of a fourth order filter consisting of two doublets. As in the former filter set-up, the in- and output couplings are realized as inductive plates with defined height, width and distance to the ceramic. Once again, four screws from the sidewalls are used to tune the dual-mode resonators similar to the basic set-up from Fig. 2. The coupling between both doublets is realized in form of a T-shaped iris aperture with width  $w_i$  and height  $h_i$  ( $i = 1, 2$ ). The shape of the aperture is adopted from the shape of the ceramics as well as the coupling fields [19].

Due to multiple cross-dependencies that occur when the filter is tuned, a direct synthesis method is not available. As a design guideline for the synthesis of a fourth order filter with one TZ below and one TZ above the passband, the initial tuning screw depths from the doublets in Fig. 5(a) and (b) can be used. The dimensions of the blend aperture can again be estimated by coupling matrix extraction techniques.

Exemplary, a coupling matrix of a fourth order filter with two TZs is shown in Table 2. The topology of the coupling matrix is visualized in Fig. 15(b). The input and output couplings both excite two modes in the Y-shaped ceramic, while

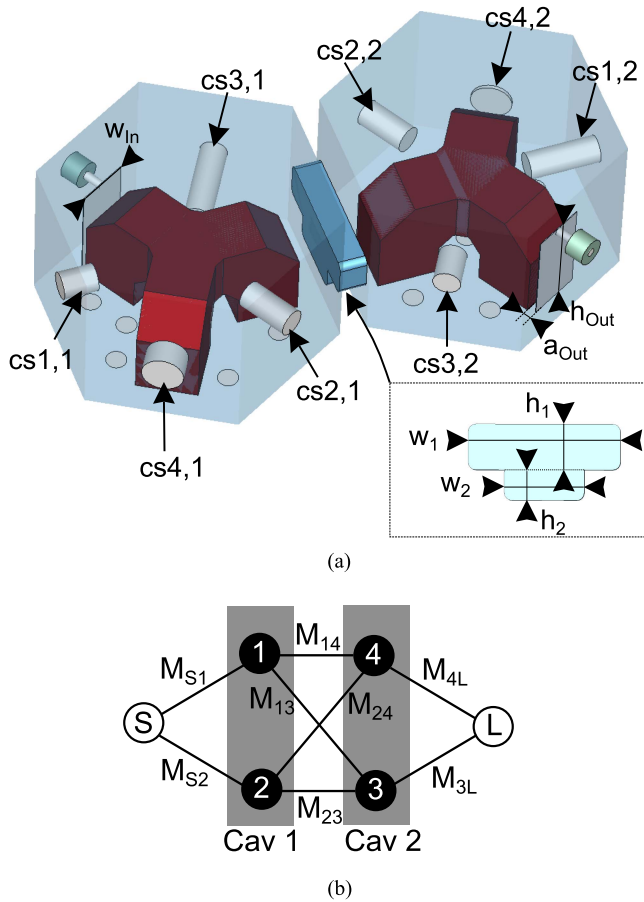


**FIGURE 15.** (a) Simulation model of a fourth order filter consisting of two coupled Y-shaped ceramics and (b) corresponding coupling topology.

**TABLE 2.** Coupling Matrix of the Filter Topology in Fig. 15 (b) With TZs at Normalized Frequencies  $f_{TZ,LP} = [-j1.488, j2.44]$  and a Return Loss Level of  $RL = 20$  dB

-	S	1	2	3	4	L
S	0.0	0.543	-0.866	0.0	0.0	0.0
1	0.543	1.134	0.0	0.182	0.103	0.0
2	-0.866	0.0	-0.481	0.636	0.359	0.0
3	0.0	0.182	0.636	0.623	0.0	-0.808
4	0.0	0.103	0.359	0.0	-1.104	0.626
L	0.0	0.0	0.0	-0.808	0.626	0.0

one coupling factor is assumed to be positive and the other one is negative. The position of the TZs is mainly determined by the sign of the self-couplings: The first doublet produces a TZ below the passband ( $M_{11} > M_{22}$ ) while the second doublet generates a TZ above the passband ( $M_{33} > M_{44}$ ). In the topology in Fig. 15(b), which represents the coupling matrix in Table 2, four coupling factors between the first / second as well as third / fourth resonance exist, which cannot be influenced individually. Fig. 16 shows a plot of these coupling factors in dependency from the iris width  $w_1$ , which is varied between 18 mm to 22 mm. A nearly linear dependency between the coupling factors and the iris width can be observed.

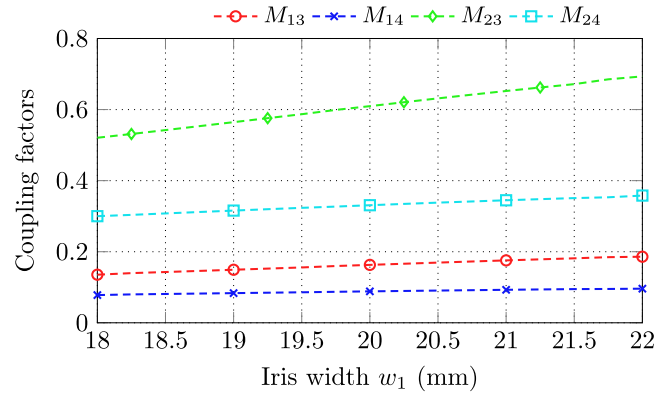


**FIGURE 16.** Coupling factors of the filter topology in Fig. 15 (b) in dependency from the iris width  $w_1$  (compare Fig. 15 (a)).

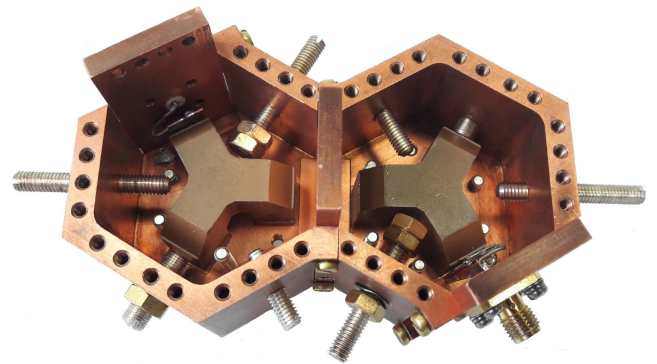


**FIGURE 17.** Prototype consisting of two coupled Y-shaped resonator segments as shown in Fig. 10 (covers removed).

Using the coupling matrix as a guideline, it is possible to estimate the width of the iris accordingly.

The final dimensions of the iris aperture, suitable tuning screw depths as well as the dimensions of the input / output coupling are found using optimization strategies in CST microwave studio. Two measurements are accomplished using the housing presented in the former section. The prototype is depicted in Fig. 17.

## B. MEASUREMENT RESULTS

The measurement results are shown in Figs. 18 and 19. In order to obtain a meaningful starting point for the tuning process, one resonator is tuned in agreement with Fig. 5(a), while the depths of all tuning screws of the second resonator can be adopted from Fig. 5(b). After tuning, the filter reveals a nearly symmetric pair of TZs at normalized frequencies  $f_{TZ,LP,1} = -j2.17$  and  $f_{TZ,LP,2} = j2.22$  as well as a return loss level of  $RL = 20$  dB (compare Fig. 18). An unloaded Q-factor of  $Q_u \approx 1350$  can be estimated. In Fig. 19 measurement results are presented, in which both TZs are placed above the passband at normalized frequencies  $f_{TZ,LP,1} = j1.55$  and  $f_{TZ,LP,2} = j2.89$ . It is not required to replace the centered iris aperture, only the depths of the tuning screws need to be varied. The filter can be matched to a return loss level



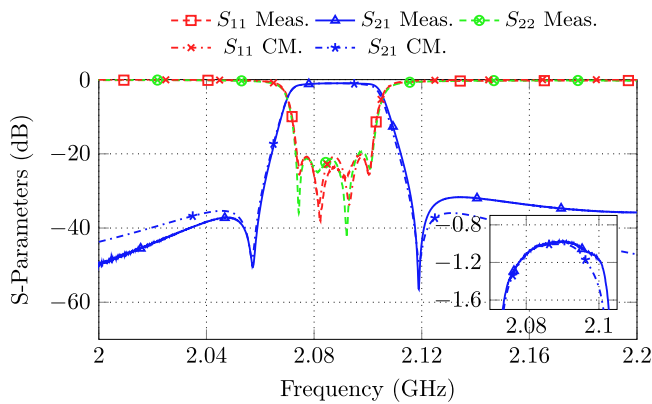


**FIGURE 18.** Measurement results of the prototype in Fig. 17 with a TZ below and a TZ above the passband in comparison to the coupling matrix representation in Table 4.

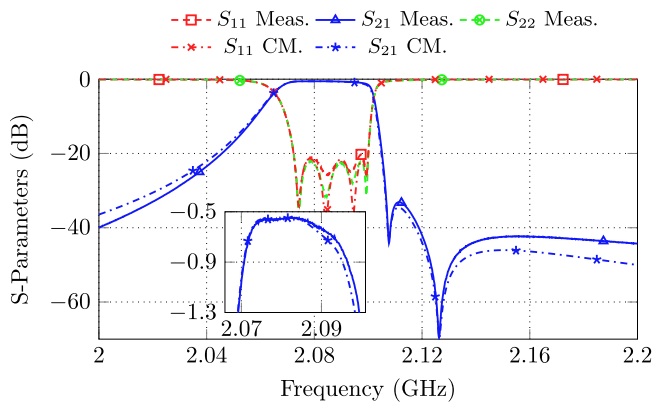


**FIGURE 19.** Measurement results of the prototype in Fig. 17 with two TZs above the passband in comparison to the coupling matrix representation in Table 5.

of  $RL = 21$  dB and reveals a higher unloaded Q-factor of  $Q_u \approx 2200$  compared to the first measurement. The differences in the unloaded quality factors must be associated with variations in the quality of the clamping of the resonators and the assembly of the filter. The spurious mode performance is shown in Fig. 20. The first spurious mode is located at 2577 MHz.

The Q-factor, especially of the first measurement, is comparatively low and can be increased for practical applications by the following adaptations:

- The modular set-up is a cost-efficient approach to realize multiple filter set-ups without manufacturing many components. However, due to multiple transitions, the Q-factor is reduced and a fixed set-up should be used for commercial / industrial purposes.
- The Y-shaped ceramics can be soldered to the housing, if the operating environment does not have high temperature fluctuations. Alternatively, the retaining screws should consist of a material which is proven to have low losses.

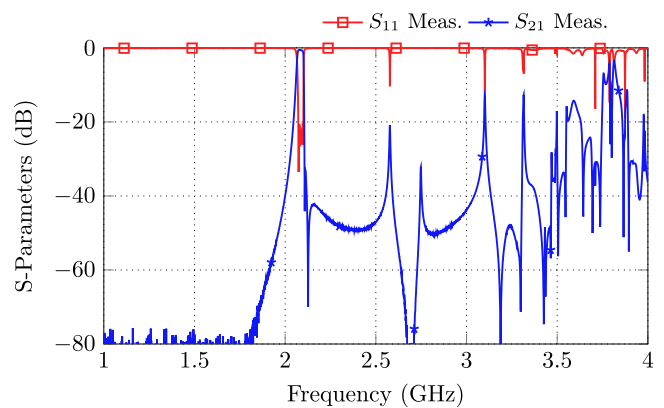


**FIGURE 20.** Spurious mode performance of the measurement results from Fig. 19.

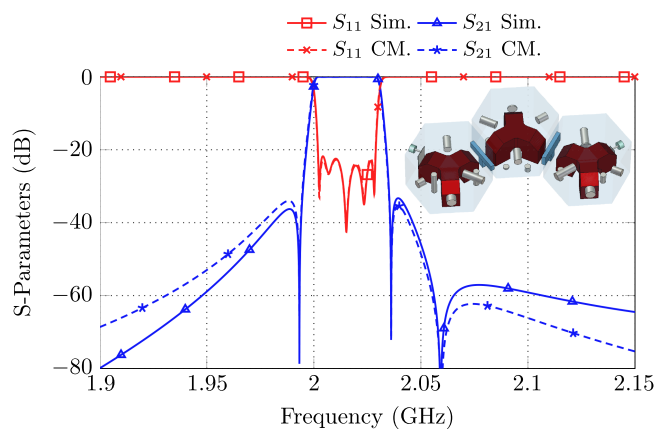


**FIGURE 21.** Simulation results of a sixth order filter consisting of three coupled doublets in comparison to the coupling matrix representation in Table 6. The inset shows the simulation model.

- The tuning screws from the sidewalls are inserted very deeply. Alternatively, the ceramic might be manufactured to have holes in the feet in each of the three branches, in which tuning screws might be inserted instead.

As a further extension of the results presented above, Fig. 21 shows the simulation results of a sixth order filter consisting of three doublets. In this case two TZs are placed above the passband and one TZ is localized below. As discussed above, a direct synthesis approach is not available yet and the presented results are based on optimization of the structure shown in the inset. Additionally, the tuning screws from the bottom were considered and used in this simulation.

### C. TEMPERATURE STABILITY

A temperature stability analysis of the filter in Fig. 17 is performed in order to obtain information about thermal drift. For this investigation, the configuration in Fig. 19 with two TZs placed above the passband is used. The temperature is varied in a range between  $-20^\circ$  C and  $+75^\circ$  C. The results are shown in Fig. 22. The center frequency is downshifted from

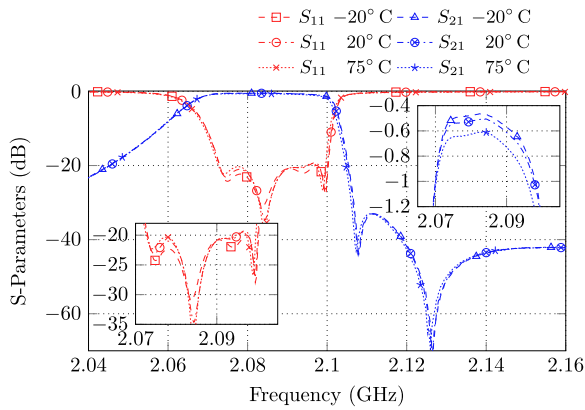


**FIGURE 22.** Temperature stability analysis of the filter in Fig. 17.

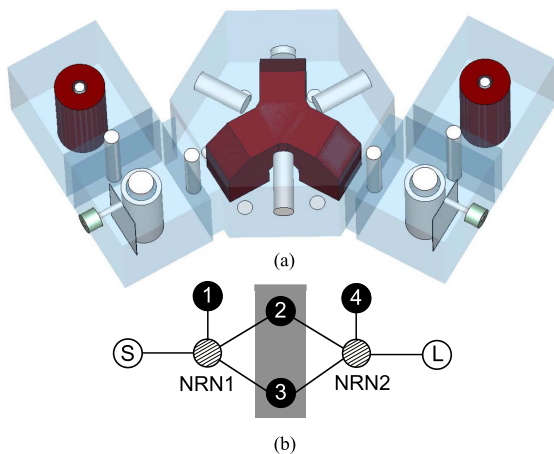


**FIGURE 23.** (a) Simulation set-up of a fourth order filter consisting of a doublet as well as two extracted pole segments and (b) corresponding coupling topology.

2086.6 MHz at  $-20^{\circ}\text{C}$  to 2086.11 MHz at  $75^{\circ}\text{C}$ . The center frequency therefore varies with  $-5.16\text{ kHz/K}$  (corresponding to 2.472 ppm). Furthermore, the insertion loss slightly increases with increasing temperature.

### V. COMBINATION OF THE DOUBLET WITH EXTRACTED POLE SEGMENTS

A further approach for the incorporation of TZs in a filter response by avoiding (negative) cross-coupling apertures is given by the extracted pole technique [23], [24]. An extracted pole segment consists of a non-resonating node (NRN), which is solely coupled to a single resonator. Such a segment is able to introduce a reflection zero as well as a TZ.

A fourth-order prototype consisting of a Y-shaped ceramic and two extracted pole resonators is shown in Fig. 23(a), while the topology is depicted in (b). In total three TZs are generated. Two of which are realized by the extracted pole segments, which are indicated as a combination of an NRN coupled to a dangling resonator (resonator one and four). The third TZ is realized by the Y-shaped ceramic. While all resonating nodes are realized by dielectric resonators, the NRNs

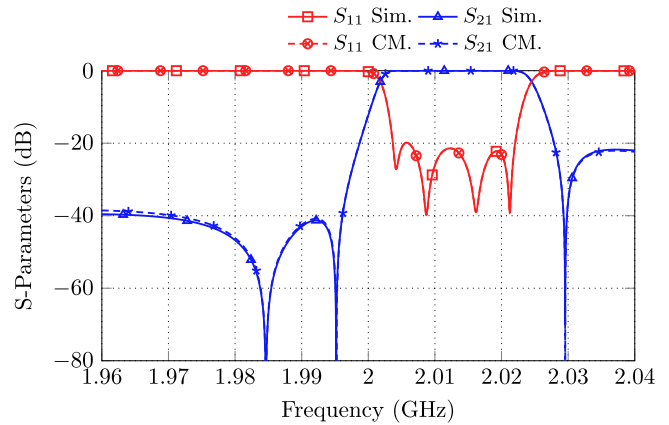


**FIGURE 24.** Simulated S-Parameters of the model from Fig. 23 in comparison to the S-Parameters generated from the coupling matrix in Table 3.

**TABLE 3.** Coupling Matrix of the Model/Topology From Fig. 23(a)/(b) for the Realization of the S-Parameter Response in Fig. 24

-	S	N1	1	2	3	4	N2	L
S	0.0	1.0	0.0	0.0	0.0	0.0	0.0	0.0
N1	1.0	2.44	2.46	0.41	-0.68	0.0	0.0	0.0
1	0.0	2.46	2.41	0.0	0.0	0.0	0.0	0.0
2	0.0	0.41	0.0	-1.02	0.0	0.0	0.41	0.0
3	0.0	-0.68	0.0	0.0	0.21	0.0	0.69	0.0
4	0.0	0.0	0.0	0.0	0.0	1.44	1.43	0.0
N2	0.0	0.0	0.0	0.41	0.69	1.43	1.44	1.0
L	0.0	0.0	0.0	0.0	0.0	0.0	1.0	0.0

are implemented as coaxial resonators [27]. These resonators are detuned with respect to the center frequency of the filter and therefore show a reactance at the filter center frequency as desired in the extracted pole approach.

It is not necessarily required to use coaxial resonators as NRNs. However, this type of resonator often shows a superior spurious mode performance as well as a large tuning range [6], [28]. The S-Parameter response is shown in Fig. 24. The TZs below the passband are realized by the extracted pole segments close to the source / load port of the filter whereas the centered Y-shaped ceramic generates the TZ above the passband.

The corresponding coupling matrix for this approach is shown in Table 3 and was obtained by optimization. Furthermore, as each NRN introduces an additional degree of freedom in the coupling matrix representation, the input and output coupling strength was set to unity [29].

### VI. CONCLUSION

This paper describes the usage of Y-shaped ceramics as doublet structures in higher order filters and different coupling topologies. For this purpose, the fundamental eigenmodes arising in Y-shaped ceramics are discussed firstly. The influence of tuning mechanisms in a second order filter set-up

on the coupling matrix entries are presented as well. Subsequently, fourth order filters with one or two transmission zeros are realized. The proof of concept is implemented based on a modular set-up, which allows the realization of filters composed by single TM<sub>010</sub>-mode as well as Y-shaped doublet structures. It is shown by simulations that at least three Y-shaped ceramics can be coupled with each other, allowing the implementation of a sixth order filter with three TZs. Furthermore, the doublet structure can be coupled with two extracted pole sections to create a fourth order filter with three transmission zeros. In addition, possibilities to further improve the performance of the filters are discussed in the form of fixed filter set-ups, holes in the feet of the ceramics for inserting tuning screws, and soldering the Y-shaped ceramics to the cavity.

**APPENDIX**

**TABLE 4. Coupling Matrix Representation of the S-Parameters in Fig. 18 With TZs at  $f_{TZ,LP,1} = -j2.17$  and  $f_{TZ,LP,2} = j2.22$**

-	S	1	2	3	4	L
S	0.0	0.619	-0.818	0.0	0.0	0.0
1	0.619	1.096	0.0	0.295	0.153	0.0
2	-0.818	0.0	-0.630	0.58	0.3	0.0
3	0.0	0.295	0.58	0.634	0.0	-0.816
4	0.0	0.153	0.3	0.0	-1.095	0.622
L	0.0	0.0	0.0	-0.816	0.622	0.0

**TABLE 5. Coupling Matrix Representation of the S-Parameters in Fig. 19 With TZs at  $f_{TZ,LP,1} = j1.55$  and  $f_{TZ,LP,2} = j2.89$**

-	S	1	2	3	4	L
S	0.0	0.597	-0.881	0.0	0.0	0.0
1	0.597	-1.113	0.0	0.188	0.111	0.0
2	-0.881	0.0	0.658	0.644	0.380	0.0
3	0.0	0.188	0.644	0.894	0.0	-0.809
4	0.0	0.111	0.380	0.0	-0.982	0.692
L	0.0	0.0	0.0	-0.809	0.692	0.0

**TABLE 6. Coupling Matrix Representation of the S-Parameters in Fig. 21 With One TZ Below and Two TZs Above the Passband at  $f_{TZ,LP,1} = -j1.659$ ,  $f_{TZ,LP,2} = j1.541$  and  $f_{TZ,LP,3} = j3.234$**

-	S	1	2	3	4	5	6	L
S	0.0	0.60	-0.88	0.0	0.0	0.0	0.0	0.0
1	0.60	1.12	0.0	0.12	0.19	0.0	0.0	0.0
2	-0.88	0.0	-0.59	0.35	0.56	0.0	0.0	0.0
3	0.0	0.12	0.35	-0.89	0.0	0.34	0.12	0.0
4	0.0	0.19	0.56	0.0	0.35	-0.63	-0.22	0.0
5	0.0	0.0	0.0	0.34	-0.63	0.91	0.0	-1.07
6	0.0	0.0	0.0	0.12	-0.22	0.0	-1.84	1.05
L	0.0	0.0	0.0	0.0	0.0	-1.07	1.05	0.0

**REFERENCES**

- [1] S. J. Fiedziuszko and S. Holmes, "Dielectric resonators raise your high-Q," *IEEE Microw. Mag.*, vol. 2, no. 3, pp. 50–60, Sep. 2001.
- [2] R. R. Mansour, "Filter technologies for wireless base stations," *IEEE Microw. Mag.*, vol. 5, no. 1, pp. 68–74, Mar. 2004.
- [3] J.-F. Liang and W. D. Blair, "High-Q TE<sub>01</sub> mode DR filters for PCS wireless base stations," *IEEE Trans. Microw. Theory Techn.*, vol. 46, no. 12, pp. 2493–2500, Dec. 1998.
- [4] C. Wang, H.-W. Yao, K. Zaki, and R. Mansour, "Mixed modes cylindrical planar dielectric resonator filters with rectangular enclosure," *IEEE Trans. Microw. Theory Techn.*, vol. 43, no. 12, pp. 2817–2823, Dec. 1995.
- [5] P. Boe, D. Miek, F. Kamrath, and M. Höft, "Hybrid inline TE/TM mode dielectric resonator filters with wide spurious free range and controllable transmission zeros," in *Proc. 50th Eur. Microw. Conf.*, Utrecht, The Netherlands, 2021, pp. 555–558.
- [6] M. Höft, "Bottom coupling of combline resonators for hybrid dielectric / air-cavity bandpass filters," in *Proc. Eur. Microw. Conf.*, 2006, pp. 1323–1326.
- [7] Y. Kobayashi and S. Yoshida, "Bandpass filters using TM<sub>010</sub> dielectric rod resonators," in *MTT-S Int. Microw. Symp. Dig.*, Ottawa, ON, Canada, 1978, pp. 233–235.
- [8] M. Höft and T. Magath, "Compact base-station filters using TM-mode dielectric resonators," in *Proc. German Microw. Conf.*, Karlsruhe, Germany, 2006.
- [9] L. Pelliccia et al., "Compact on-board L-band dielectric-loaded diplexer for high-power applications," in *Proc. 49th Eur. Microw. Conf.*, 2019, pp. 61–64.
- [10] V. Walker and I. Hunter, "Design of cross-coupled dielectric-loaded waveguide filters," *Proc. Inst. Elect. Eng., Microw. Antennas Propag.*, vol. 148, no. 2, pp. 91–96, Apr. 2001.
- [11] M. Höft, "Bandpass filter using TM-mode dielectric rod resonators with novel input coupling," in *IEEE MTT-S Int. Microw. Symp. Dig.*, 2009, pp. 1601–1604.
- [12] R. Snyder, S. Bastioli, and G. Macchiarella, "The extracted-zero: A practical solution for transmission zeros in wideband filters," *IEEE Microw. Wireless Compon. Lett.*, vol. 31, no. 9, pp. 1043–1046, Sep. 2021.
- [13] G. Macchiarella, S. Tamiazzo, S. Bastioli, and R. Snyder, "Synthesis of extracted-zero filters," *IEEE Microw. Wireless Compon. Lett.*, vol. 32, no. 6, pp. 644–647, Jun. 2022.
- [14] S. Amari and U. Rosenberg, "The doublet: A new building block for modular design of elliptic filters," in *Proc. 32nd Eur. Microw. Conf.*, 2002, pp. 1–3.
- [15] M. Höft, "Y-shape dielectric dual-mode resonator," *IEEE Trans. Microw. Theory Techn.*, vol. 56, no. 12, pp. 3066–3071, Dec. 2008.
- [16] M. Höft, "New concepts for dielectric multi-mode resonators with branches," in *IEEE MTT-S Int. Microw. Symp. Dig.*, 2008, pp. 727–730.
- [17] M. Höft and D. Miek, "Complex eigenmodes for modelling of dielectric dual-mode resonators," in *Proc. IEEE MTT-S Int. Conf. Numer. Electromagn. Multiphys. Model. Optim.*, 2018, pp. 1–4.
- [18] R. J. Cameron, "Advanced coupling matrix synthesis techniques for microwave filters," *IEEE Trans. Microw. Theory Techn.*, vol. 51, no. 1, pp. 1–10, Jan. 2003.
- [19] D. Miek, P. Boe, F. Kamrath, and M. Höft, "Dielectric TM dual-mode filters with Y-shape," in *Proc. IEEE MTT-S Int. Microw. Filter Workshop*, 2021, pp. 69–72.
- [20] D. Miek, P. Boe, K. Braasch, S. Simmich, F. Kamrath, and M. Höft, "Design and realization of bent Y-shaped ceramic dual-mode resonators and filters," in *Proc. IEEE 24th Int. Microw. Radar Conf.*, 2022, pp. 1–6.
- [21] U. Rosenberg and S. Amari, "Novel coupling schemes for microwave resonator filters," *IEEE Trans. Microw. Theory Techn.*, vol. 50, no. 12, pp. 2896–2902, Dec. 2002.
- [22] J.-S. Hong, *Microstrip Filters for RF/Microwave Applications*, 2nd ed., K. Chang, Ed. Hoboken, NJ, USA: Wiley, 2011.
- [23] J. Rhodes and R. Cameron, "General extracted pole synthesis technique with applications to low-loss TE<sub>011</sub> mode filters," *IEEE Trans. Microw. Theory Techn.*, vol. 28, no. 9, pp. 1018–1028, Sep. 1980.
- [24] G. Macchiarella and S. Tamiazzo, "An application-oriented design procedure for cascaded-block extracted-pole filters," *IEEE Trans. Microw. Theory Techn.*, vol. 69, no. 1, pp. 647–658, Jan. 2021.

- [25] P. Rezaee and M. Höft, "A new class of compact dual-mode dielectric resonator filters," in *Proc. IEEE MTT-S Int. Microw. Symp.*, 2016, pp. 1–3.
- [26] G. Macchiarella, "Extraction of unloaded Q and coupling matrix from measurements on filters with large losses," *IEEE Microw. Wireless Compon. Lett.*, vol. 20, no. 6, pp. 307–309, Jun. 2010.
- [27] K. Braasch, D. Miek, P. Boe, F. Kamrath, and M. Höft, "Dielectric TM mode extracted pole filters with large spurious free range," in *Proc. 51st Eur. Microw. Conf.*, London, U.K., Apr. 2022, pp. 114–117.
- [28] H.-Y. Hwang, N.-S. park, Y.-H. Cho, S.-W. Yun, and L.-S. Chang, "The design of band-pass filters made of both dielectric and coaxial resonators," in *IEEE MTT-S Int. Microw. Symp. Dig.*, 1997, pp. 805–808.
- [29] R. J. Cameron, C. M. Kudsia, and R. R. Mansour, *Microwave Filters for Communication Systems: Fundamentals, Design, and Applications*, 2nd ed. Hoboken, NJ, USA: Wiley, 2018.



**DANIEL MIEK** (Member, IEEE) was born in Minden, Germany, on January 10, 1992. He received the B.Sc. and M.Sc. degrees in electrical engineering and information technology from Kiel University, Kiel, Germany in 2015 and 2017, respectively, where he is currently working toward the Dr.-Ing. degree with the Department of Electrical and Information Engineering as a member of the Chair of Microwave Engineering. His research interests include the design, realization and optimization of waveguide, and dielectric filters.



**PATRICK BOE** (Graduate Student Member, IEEE) received the B.Sc. and M.Sc. degrees in electrical engineering, information technology, and business management from Kiel University, Kiel, Germany, in 2017 and 2019, respectively. He is currently working toward the Dr.-Ing. degree with the Department of Electrical and Information Engineering as a member of the Chair of Microwave Engineering. His research interests include the design, realization and optimization of dielectric resonator filters, and also dielectric multi-mode filters.



**FYNN KAMRATH** (Graduate Student Member, IEEE) received the B.Sc. and M.Sc. degrees in 2017 and 2019, respectively, in electrical engineering and information technology from Kiel University, Kiel, Germany, where he is currently working toward the Dr.-Ing. degree with the Department of Electrical and Information Engineering as a member of the Chair of Microwave Engineering. His research interests include the design, realization, and optimization of center frequency, and bandwidth tunable microwave filters.



**KENNET BRAASCH** received the B.Sc. and M.Sc. degrees in electrical engineering and information technology from Kiel University, Kiel, Germany, in 2018 and 2020, respectively. He is currently working toward the Dr.-Ing. degree with the Department of Electrical and Information Engineering as a member of the Chair of Microwave Engineering. His research interests include the design of a radar system for the detection and characterization of small particle streams.



**WOLFGANG TAUTE** received the Dipl.-Ing. (FH) degree in electrical engineering and information technology from the University of Applied Sciences, Emden, Germany, in 1993. He is currently working as a Laboratory Engineer with the Chair of Microwave Engineering, Department of Electrical and Information Engineering, Kiel University, Kiel, Germany. His research interests include humidity measurements in organic and anorganic materials and the construction of measurement instruments.



**MICHAEL HÖFT** (Senior Member, IEEE) was born in Lübeck, Germany, in 1972. He received the Dipl.-Ing. degree in electrical engineering and Dr.-Ing. degree from the Hamburg University of Technology, Hamburg, Germany, in 1997 and 2002, respectively. From 2002 to 2013, he joined the Communications Laboratory, European Technology Center, Panasonic Industrial Devices Europe GmbH, Lüneburg, Germany. He was a Research Engineer and then Team Leader, where he was engaged in research and development of microwave circuitry and components, particularly filters for cellular radio communications. From 2010 to 2013, he was also a Group Leader for research and development of sensor and network devices. Since October 2013, he has been a Full Professor with the Faculty of Engineering, Kiel University, Kiel, Germany, where he is currently the Head of the Microwave Group, Department of Electrical and Information Engineering. His research interests include active and passive microwave components, (sub-) millimeter-wave quasi-optical techniques and circuitry, microwave and field measurement techniques, microwave filters, microwave sensors, and magnetic field sensors. Dr. Höft is a member of the European Microwave Association (EuMA), Association of German Engineers (VDI), and German Institute of Electrical Engineers (VDE).